Crustal structure and fluid distribution beneath the southern part of the Hidaka collision zone revealed by 3-D electrical resistivity modeling

Ichihara, Hiroshi ; Mogi, Toru ; Tanimoto, Kengo ; Yamaya, Yusuke ; Hashimoto, Takeshi ; Uyeshima, Makoto ; Ogawa, Yasuo

(Citation)
Geochemistry Geophysics Geosystems,17(4):1480-1491

(Issue Date)
2016-04

(Resource Type)
journal article

(Version)
Version of Record

(URL)
https://hdl.handle.net/20.500.14094/90003516

AGU PUBLICATIONS

Geochemistry, Geophysics, Geosystems

RESEARCH ARTICLE
10.1002/2015GC006222

Key Points:
- 3-D resistivity imaging demonstrated geological and fluid distributions in the Hidaka collision zone
- Upwelling pore fluid from the subducting plate contributes to anomalously deep inland earthquakes
- The image supports an obduction model of the Kurile arc over the NE Japan arc

Supporting Information:
- Supporting Information S1

Correspondence to:
H. Ichihara,
h-ichi@maritime.kobe-u.ac.jp

Citation:
Ichihara, H., T. Mogi, K. Tanimoto, Y. Yamaya, T. Hashimoto, M. Uyeshima, and Y. Ogawa (2016), Crustal structure and fluid distribution beneath the southern part of the Hidaka collision zone revealed by 3-D electrical resistivity modeling, *Geochem. Geophys. Geosyst.*, *17*, 1480–1491, doi:10.1002/2015GC006222.

Received 10 DEC 2015
Accepted 28 MAR 2016
Accepted article online 31 MAR 2016
Published online 29 APR 2016

Crustal structure and fluid distribution beneath the southern part of the Hidaka collision zone revealed by 3-D electrical resistivity modeling

Hiroshi Ichihara[1], Toru Mogi[2], Kengo Tanimoto[3], Yusuke Yamaya[4], Takeshi Hashimoto[2], Makoto Uyeshima[5], and Yasuo Ogawa[6]

[1]Graduate School of Maritime Sciences, Kobe University, Kobe, Japan, [2]Institute of Seismology and Volcanology, Hokkaido University, Sapporo, Japan, [3]Formerly Institute of Seismology and Volcanology, Hokkaido University Sapporo, Japan, [4]National Institute of Advanced Industrial Science and Technology, Koriyama, Japan, [5]Earthquake Research Institute, University of Tokyo, Tokyo, Japan, [6]Volcanic Fluid Research Center, Tokyo Institute of Technology, Tokyo, Japan

Abstract The Hidaka collision zone, where the Kurile and northeastern (NE) Japan arcs collide, provides a useful study area for elucidating the processes of arc-continent evolution and inland earthquakes. To produce an image of the collision structure and elucidate the mechanisms of anomalously deep inland earthquakes such as the 1970 Hidaka earthquake (M6.7), we conducted magnetotelluric observations and generated a three-dimensional resistivity distribution in the southern part of the Hidaka collision zone. The modeled resistivity was characterized by a high resistivity area in the upper crust of the Kurile arc corresponding to metamorphic rocks. The model also showed conductive zones beneath the center of the collision zone. The boundary between the resistive and conductive areas corresponds geometrically to the Hidaka main thrust, which is regarded as the arc-arc boundary. The correspondence supports the collision model that the upper-middle part of crust in the Kurile arc is obducting over the NE Japan arc. The conductive areas were interpreted as fluid-filled zones associated with collision processes and upwelling of dehydrated fluid from the subducting Pacific slab. The fluid flow possibly contributes to over-pressurized conduction that produces deep inland earthquakes. We also observed a significant conductive anomaly beneath the area of Horoman peridotite, which may be related to the uplift of mantle materials to the surface.

1. Introduction

The southern part of Hokkaido Island, northern Japan, is situated on the triple junction of the northeastern (NE) Japan and Kurile arcs and the subducting Pacific plate (Figure 1a). The westward migration of the Kurile fore-arc sliver caused by the oblique subduction of the Pacific plate has formed the Hidaka collision zone (HCZ) along the boundary between the NE Japan and Kurile arcs since the middle Miocene [e.g., *Kimura*, 1986]. In the HCZ, the Kurile forearc sliver has obducted over the NE Japan arc along the Hidaka main thrust (HMT), which expose metamorphic and intrusive rocks formed in the middle-upper crust at the surface of the Kurile arc (the Hidaka metamorphic belt). Because the metamorphic rock sequence reveals a section of continental-type crust [e.g., *Komatsu et al*., 1983], the HCZ provides a useful study area for investigating the evolution of continental and island arc crust. In addition, an unaltered ultra-mafic rock body, Horoman peridotite, is exposed on the west side of the Hidaka Metamorphic Belt (Figure 1b), which reveals the characteristics of mantle rocks [e.g., *Takahashi*, 1992].

The HCZ is also an important area for studying inland earthquakes. The 1970 Hidaka earthquake (M6.7) occurred in the southern part of the HCZ (Figure 1b). The focal area was estimated at the depth range between 15 and 35 km based on aftershock observations [*Moriya*, 1972]. This depth is anomalously deep for an inland earthquake because the seismogenic area generally does not reach to the lower crust where rock deforms plastically [e.g., *Scholz*, 2002]. Thus, studying the focal area of the earthquake will contribute to understanding the conditions for brittle fault failure in inland areas.

Electrical resistivity profiling has provided insights into the tectonic processes in collision zones [*Bertrand et al*., 2012; *Unsworth*, 2010]. In addition, imaging of the resistivity distribution has facilitated elucidation of

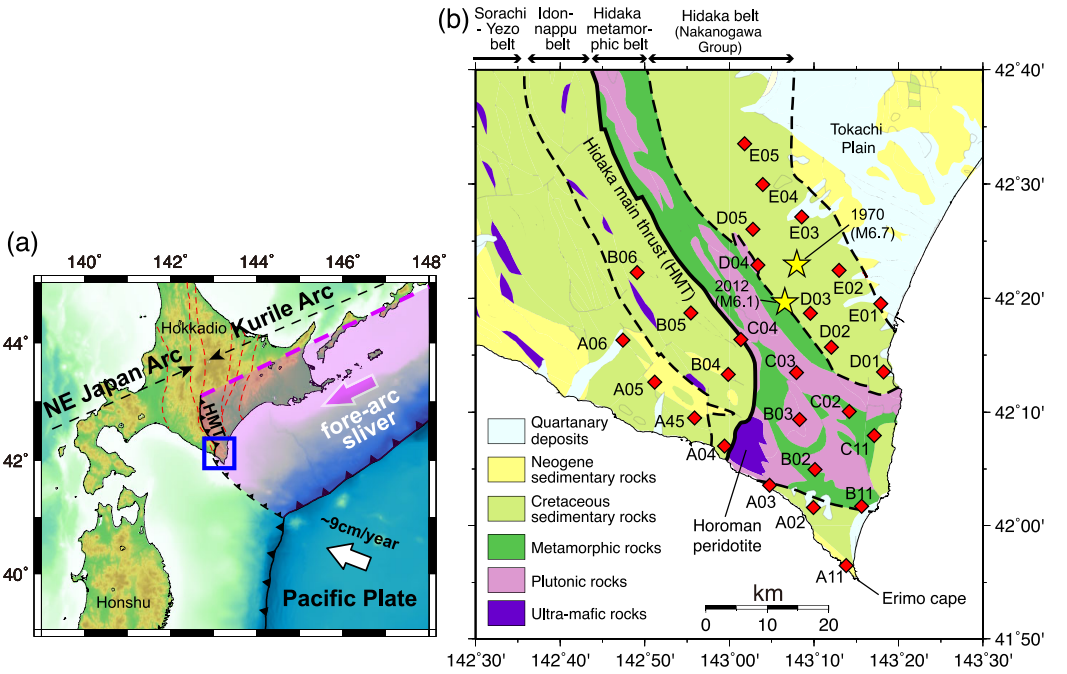

Figure 1. Study location with topographic map. (a) Location of study area with tectonic boundaries. Red dashed lines denote tectonic boundaries based on *Kimura* [1994]. The blue rectangle denotes the location of Figure 1b. "HMT" indicates Hidaka Main Thrust. (b) Location of MT stations with a simplified geological map based on the *Geological Survey of Japan* [2007]. Red diamonds denote MT stations. Yellow stars denote epicenters of the 1970 Hidaka (M6.7) and 2012 earthquakes (M6.1).

the mechanisms of earthquake generation because the resistivity is highly dependent on the pore-fluid distribution, which controls the behavior of the fault rupture [*Becken and Ritter*, 2012; *Ichihara et al*., 2011; *Sibson*, 2014; *Wannamaker et al*., 2009]. In the northern part of the HCZ, *Ogawa et al*. [1994] generated a rough image of the resistivity distribution based on wideband magnetotelluric (MT) surveys and two-dimensional (2-D) forward resistivity modeling. The authors concluded the existence of a high-resistivity zone around the HMT and a steeply dipping conductive area fringing on the west side of the resistive zone. However, no surveys have been conducted in the southern part of the HCZ, where the 1970 Hidaka earthquake occurred, because the marked three-dimensionality of the resistivity distribution such as an area surrounded by conductive seawater has prevented the application of conventional 2-D resistivity modeling. However, recent progress in three-dimensional (3-D) inversion methods for MT data now enables the modeling of resistivity patterns even in such geoelectrically complex areas. Thus, we performed wideband and long-period MT surveys in the southern part of the HCZ, and estimated the resistivity distribution based on 3-D inversion procedures.

2. Magnetotelluric (MT) Measurements and Impedances

We conducted wideband and long-period MT surveys in the southern part of the HCZ in 2004. Two horizontal components of the electric field and three components of the magnetic field were obtained at 27 sites for both surveys (Figure 1b). Every measurement site was occupied with both the wideband and long-period instruments. In the wideband survey, time series were recorded for 3–7 days using an MTU2000 system (Phoenix Geophysics, Ltd., Toronto, Canada). The electric and magnetic fields were measured using Pb–$PbCl_2$ electrodes and induction coils, respectively. The time series were converted into frequency-domain MT impedance tensors and geomagnetic transfer functions between 0.00313 and 1820 s using an SSMT200 software (Phoenix Geophysics, Ltd.). The remote reference technique [*Gamble et al*., 1979] was applied to estimate the MT impedances using horizontal magnetic field data from Esashi station operated by the Geospatial Information Authority of Japan located approximately 400 km south-southwest from the study area. These processes yielded high-quality MT responses and geomagnetic transfer functions without long-period responses ($>$ 900 seconds). In the surveys for long-period data, time series were recorded using a

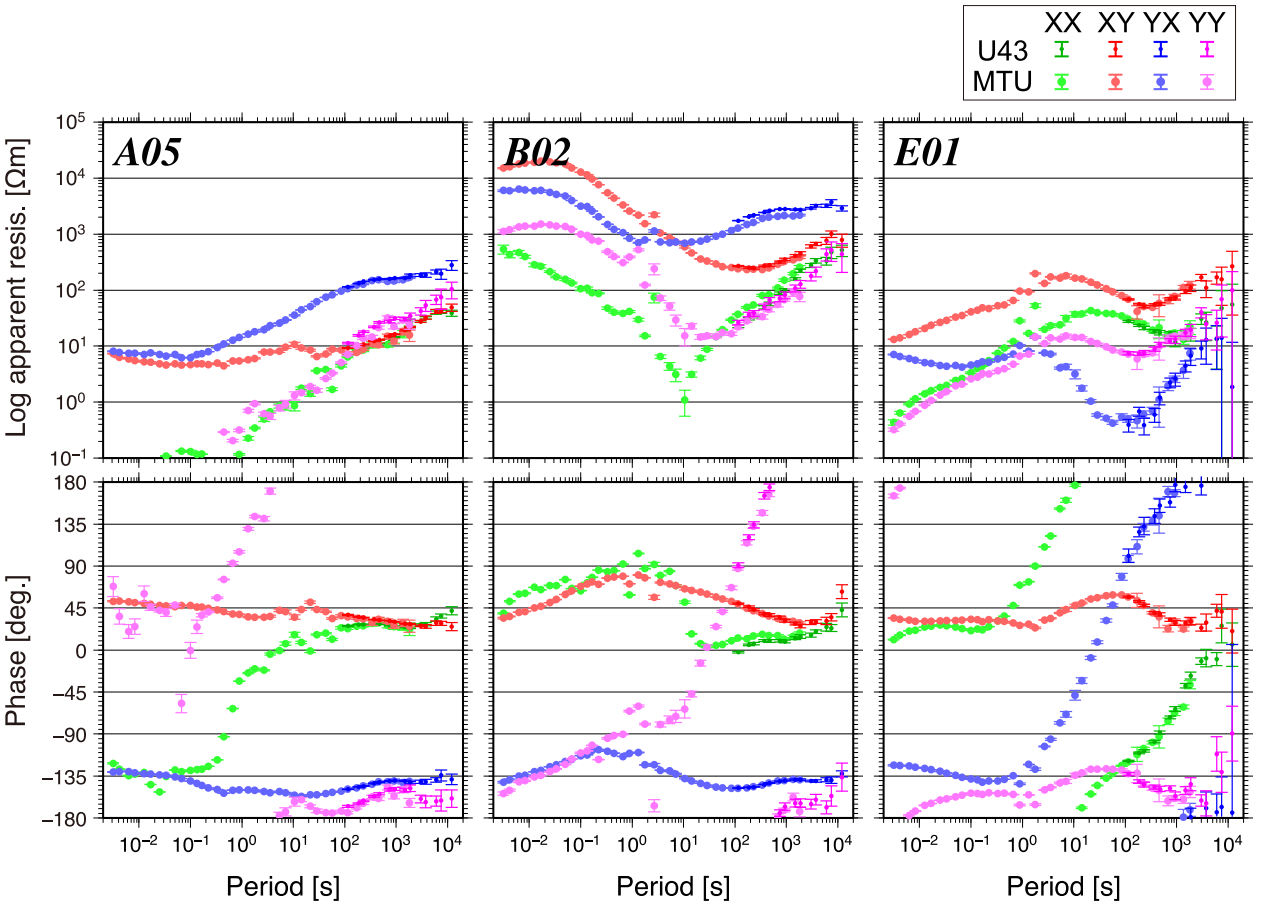

Figure 2. Sounding curves of observed apparent resistivity and impedance phases based on time series acquired using MTU2000 and U43 systems.

U43 system (Tierra Tecnica Ltd., Tokyo, Japan) for 1 month after the wideband measurements. We used the same electrode arrangements as for the wideband survey, but replaced the data logger and magnetic sensors into the U43 logger and fluxgate magnetometer, respectively. Based on the time series, we estimated the MT impedance tensors and geomagnetic transfer functions between 116 and 12,000 s using the bounded influence remote-reference processing code [*Chave and Thomson*, 2004]. Horizontal magnetic field data from Memanbetsu geomagnetic observatory (operated by the Japan Meteorological Agency) were used for remote reference processing.

The MT impedances from the wideband and long-period surveys showed almost identical sounding curves in the overlapping period range between 116 and 1,820 s, except for site D01 (Figure 2 and supporting information S1). The estimated errors of the long-period impedances were significantly smaller than those of the wideband impedances for most sites. Thus, we adopted the impedances based on the long-period surveys for the overlapped period bands. The combined MT impedances of the wideband and long-period data presented high-quality sounding curves in the period range between 0.00313 and 12,000 s at most of the MT sites (Figure 2 and supporting information S1). The curves showed the following features: (1) the shape of the curves differed significantly from site to site, implying strong heterogeneity in the resistivity distribution in this area; (2) the apparent resistivity was generally high ($>$ 1000 Ωm) at the sites on the Hidaka Metamorphic Belt. (3) The phase of the off-diagonal components of the MT impedance had anomalous values beyond the ordinal quadrant (0 to 90 and -180 to -90 degrees for the XY and YX components, respectively) at the site B01, D01, D04, D05 and E01. The phase began to increase from 1 s toward longer periods, and exceeded the phase of the ordinal quadrat by $>$100 s. Such an anomalous phase pattern, which is commonly observed in island arcs, implies strong 3-D resistivity heterogeneity [*Aizawa et al*., 2014; *Ichihara and Mogi*, 2009; *Ichihara et al*., 2013, 2014].

Next, we discuss the dimensionality of the resistivity structure based on the phase tensor ellipses [*Caldwell et al*., 2004]. The phase tensor is derived from the MT impedance tensor as:

$$\mathbf{\Phi}=\mathbf{X}^{-1}\mathbf{Y}, \tag{1}$$

where X and Y are the real and imaginary parts of the impedance tensor, respectively. While the MT impedance is often distorted by localized superficial heterogeneity in the resistivity (so-called galvanic distortion), the MT phase tensor is independent of any such distortion and can be graphically represented as an ellipse; the ellipse axes show the orientation and relative magnitude of the tensor principal values, Φ_{max} and Φ_{min}. The magnitude and orientation of the principal values visualize resistivity gradients. The geometric mean of the principal values ($\Phi_2 = (\Phi_{max}\Phi_{min})^{1/2}$) indicates the magnitude of the phase tensor response. In simple (quasi-one-dimensional) situations, decreasing resistivity with increasing depth is indicated by values of $\Phi_2 > 45°$. A third coordinate invariant parameter of the phase tensor, the skew angle β, represents the asymmetry in the phase response. The absolute value of β, $|\beta|$, is large when the resistivity structure is 3-D. Figure 3 shows the phase tensor ellipses. The azimuths of the main axes of the phase tensor ellipses are dominantly directed toward N35°W–S35°E in the long periods ($>$ 234 s in Figure 3). This azimuth is parallel to the geological boundary in the southern part of the HCZ (Figure 1b). In contrast, the phase tensor ellipses are locally varied in the shorter periods. For example, the main axes are oriented to N55°E–S55°W around the northeastern margin of Hidaka metamorphic rock in 0.885 s, implying resistivity boundary along the margin. $|\beta|$ has high values ($>$ 10°) at more than half of the MT sites in all periods, indicating that the resistivity distribution is highly 3-D. High values of Φ_2 (51–57°) and Φ_{min} ($>$ 45°, not shown in figures) occur at the sites on the NE side of the MT array where the Hidaka belt is distributed (Figure 1b), implying that resistivity decreases with depth beneath the Hidaka belt. In addition, exceptionally high Φ_2 ($>$ 60°) values are observed at sites near the Horoman peridotite in the short periods (0.885 s), implying a sharp decrease in resistivity with depth beneath this area.

3. 3-D Resistivity Inversion

The 3-D resistivity distribution was estimated based on the WSINV3D code [*Siripunvaraporn et al*., 2004], which adopts a data-space variant of Occam's approach based on *Siripunvaraporn and Egbert* [2000]. In the inversion procedure, the objective function defined as follows is minimized:

$$W_\lambda(\mathbf{m})=(\mathbf{m}-\mathbf{m}_p)^T\mathbf{C}_\mathbf{m}^{-1}(\mathbf{m}-\mathbf{m}_p)+\lambda^{-1}\left\{(\mathbf{d}-\mathbf{F}[\mathbf{m}])^T\mathbf{C}_\mathbf{d}(\mathbf{d}-\mathbf{F}[\mathbf{m}])\right\}, \tag{2}$$

where $\mathbf{m}$ and $\mathbf{m}_p$ are the model parameters and prior model vectors, respectively. $\mathbf{C}_\mathbf{m}$ is the model covariance matrix characterizing the expected magnitude and smoothness of resistivity variations relative to $\mathbf{m}_p$. $\mathbf{d}$ is the data parameter vector consisting of the observed MT impedances. $\mathbf{F}[\mathbf{m}]$ is the vector of the forward response to $\mathbf{m}$. λ is a hyperparameter that balances the data misfit and model roughness terms. $\mathbf{C}_\mathbf{d}$ is a data covariance matrix consisting of the observation errors.

We used the MT impedances at 12 periods between 0.885 and 1875 s as the data parameter ($\mathbf{d}$) for the inversion. The impedances were rotated to the azimuth of the model geometries, where the *x*- and *y*-axes were aligned along N35°E and S55°E, respectively. Error floors of 10% and 20% were applied for the off-diagonal and diagonal components, respectively. The resistivity model space covered the region of 3,336 (*x*-axis) $\times$ 3,306 (*y*-axis) $\times$ 1,415 (*z*-axis, without air layers) km discretized into 59 $\times$ 44 $\times$ 31 layers. The length and width of the blocks within the survey area were 2 km, but these widened outside the study area.

The inversion procedure began with a homogeneous half-space model consisting of 100 Ωm blocks except for the area of seawater for which the model blocks were fixed to 0.3 Ωm. The same model was adopted as a prior model ($\mathbf{m}_p$). We iterated the inversion procedure 10 times with fixed $\mathbf{m}_p$. We adopted the model with the minimum root mean square (RMS) misfit as $\mathbf{m}_p$ and the initial model of the next inversion procedure. We repeated this inversion process three times to obtain the minimum RMS misfit model (RMS misfit: 1.065). The model-predicted sounding curves of the inverted model mostly explained the measured curves (Figure 4 and supporting information Figure S2). The model-predicted phase tensors from the inverted model also explained the trend of the measured phase tensor (Figure 3).

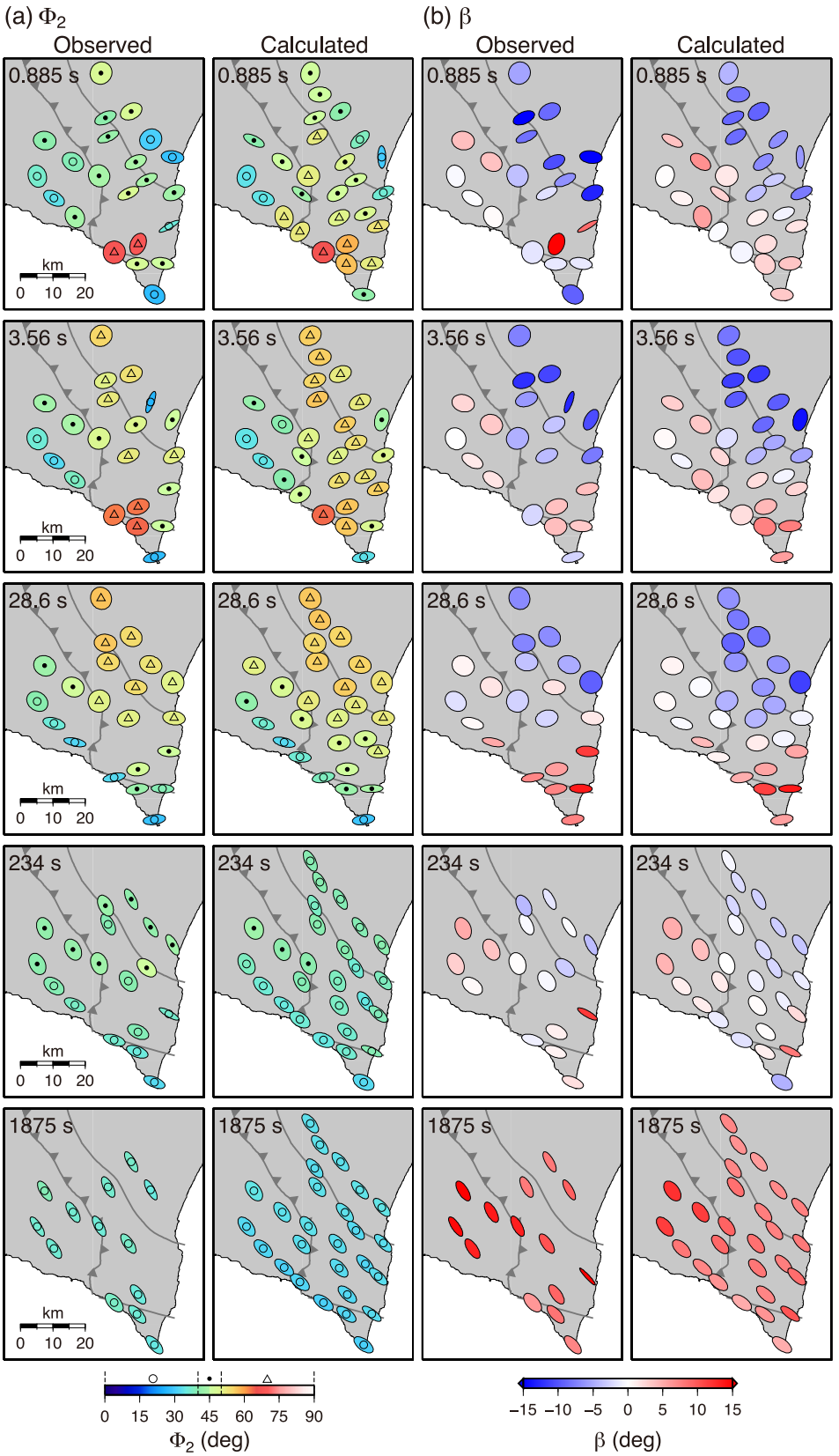

Figure 3. Phase tensor ellipses. Colored ellipses indicate for (a) Φ_2 and (b) β, respectively. Observed data with large errors were not shown in the figure ($>5°$ for Φ_2 and $2°$ for β). The model-predicted (calculated) phase tensors based on the inverted model are also shown.

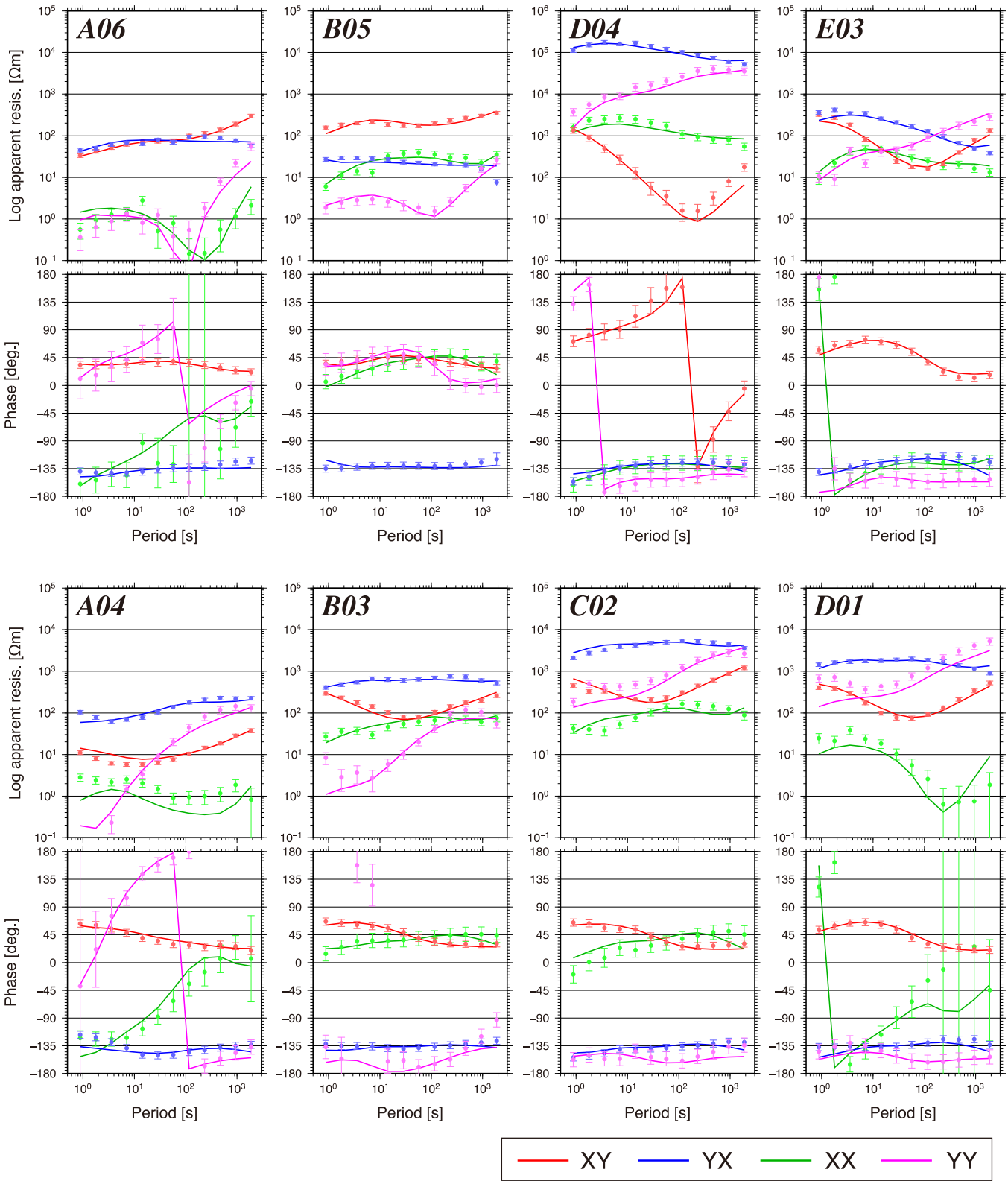

Figure 4. Observed (dots) and model-predicted (lines) sounding curves based on the inverted model. The positive directions of the *x*- and *y* axes are along N35°E and S55°E, respectively.

The inverted model showed significant resistivity variations in the study area (3–100,000 Ωm; Figures 5 and 6). The features of the resistivity model were as follows: (1) a high-resistivity zone over 3,000 Ωm (R-1) occurred beneath the Hidaka Metamorphic Belt. A sensitivity test confirmed the high resistivity in this area. When R-1 (> 1,000 Ωm) was filled with 1,000 Ωm, the model-predicted impedances changed significantly and thus did not explain the observed impedances (supporting information Figure S3); e.g., high apparent resistivity in the YX component and out-of-quadrant phase in the XY component at site D04. (2) A relatively low-resistivity zone (30–300 Ωm, C-1a) was revealed beneath R-1. The impedances required this zone because the model-predicted impedances changed significantly if the area of C-1a was allocated a uniform resistivity of 3000 Ωm (supporting information Figure S4). A vertically elongated conductor (30–300 Ω m, C-1b) was revealed in the western section of R-1 and over C-1a. C-1b was also verified based on a sensitivity test in which the area of C-1b was given a uniform resistivity of 3,000 Ωm (supporting information Figure S5). (3) A distinct conductor (3–30 Ω m, C-2) occurred at a depth of 1–5 km beneath the outcrop of Horoman peridotite. The high phase tensor value ($\Phi_2 > 60^\circ$) around the Horoman peridotite requires the conductive anomaly of C-2 (Figure 3). A sensitivity test in which the area of the C-2 was given a uniform resistivity of 1000 Ωm also supported the C-2 conductor (supporting information Figure S6). (4) Surface conductors C-3, C-4 and C-5 (3–30 Ωm) occurred on the western side, in the central area and on the eastern side of the MT array, respectively. The impedances showing low apparent resistivity and high phase in the short period bands in these areas required the surface conductors C-3, C-4, and C-5 (e.g., sites A06, B05, and E03, respectively, in Figure 4 and supporting information Figure S1). These surface conductors were also verified based on sensitivity tests in which the areas of C3, C4 and C-5 were filled with a uniform resistivity of 1,000 Ωm (supporting information Figures S7–S9, respectively).

4. Discussion

4.1. Interpretations of the Resistivity Distribution

4.1.1. Metamorphic Rocks in the Kurile Arc (R-1)

Inverted resistivity model shows excellent correlation between R-1 and the Hidaka Metamorphic Belt at shallow depth (Figures 1b, 5, 6, and 7b). Laboratory measurement showed that the resistivity of granulite sampled in the area of the MT sites between B05 and D05 was 3,000–100,000 Ωm under the upper-middle crust conditions [*Fuji-ta et al*., 2004]. Because the granulite is distributed from the surface to the middle crust in the Hidaka Metamorphic Belt [e.g., *Kimura*, 1986; *Osanai et al*., 1986], the existence of the granulite explains the resistivity of R-1 (> 3000 Ωm) and its model feature. On the other hand, *Kita et al*. [2012] discussed that the high seismic velocity zones (P-wave velocities of 7.8–8.5 km/s and S-wave velocities of 4.5–4.8 km/s) in the R-1 area were consist with seismic velocities of Horoman peridotite. Thus deep extension of the Horoman peridotie is possibly constituent of the R-1. Seismic reflection surveys found east-dipping reflection planes, which corresponded to the HMT, beneath the Hidaka metamorphic belt [*Arita et al*., 1998; *Ito*, 2000; *Iwasaki et al*., 1998, 2004; *Tsumura et al*., 1999], which displayed the obduction structure of the Kurile arc over the NE Japan arc (Figure 7a). The lower and western boundary of R-1 was coincident with the reflection boundary (Figure 7b). Therefore, R-1 can be interpreted as Hidaka metamorphic rocks and its distribution confirms an obduction structure along the HMT.

4.1.2. Upwelling Fluid Flow From the Subducting Pacific Plate (C-1a and C-1b)

A transition from basalt to eclogite occurs due to the subduction of oceanic crust associated with dehydration. In the NE Japan arc, the transition occurs from a depth of 50 km in the oceanic crust of the subducting Pacific plate and forms aqueous pore fluid-rich areas [*Hacker et al*., 2003]. The fluid-rich areas have also been indicated in the subducting oceanic crust beneath the Kurile arc based on low P-wave velocity anomalies [*Shiina et al*., 2014]. In general, saline water in the rock pores dramatically reduces the bulk resistivity of rocks. Thus, a probable cause of the C-1a zone in the subducting Pacific plate is the high pore fluid content area due to dehydrating prograde metamorphism reactions. The C-1a zone above the plate boundary and C-1b was interpreted as a fluid-rich area due to upwelling fluid from the dehydration zone based on the following reasons: (1) the collision process between the NE Japan and the Kurile arc probably forms fractured zones in this area, which generally increases the rock permeability; and (2) *Kita et al*. [2010, 2012, 2014] reported a low S-wave velocity anomaly and a significant seismic attenuated zone in this area. Thus, C-1a and C-1b indicate a pathway of upwelling fluid through the center of the HCZ from the plate boundary (Figure 8).

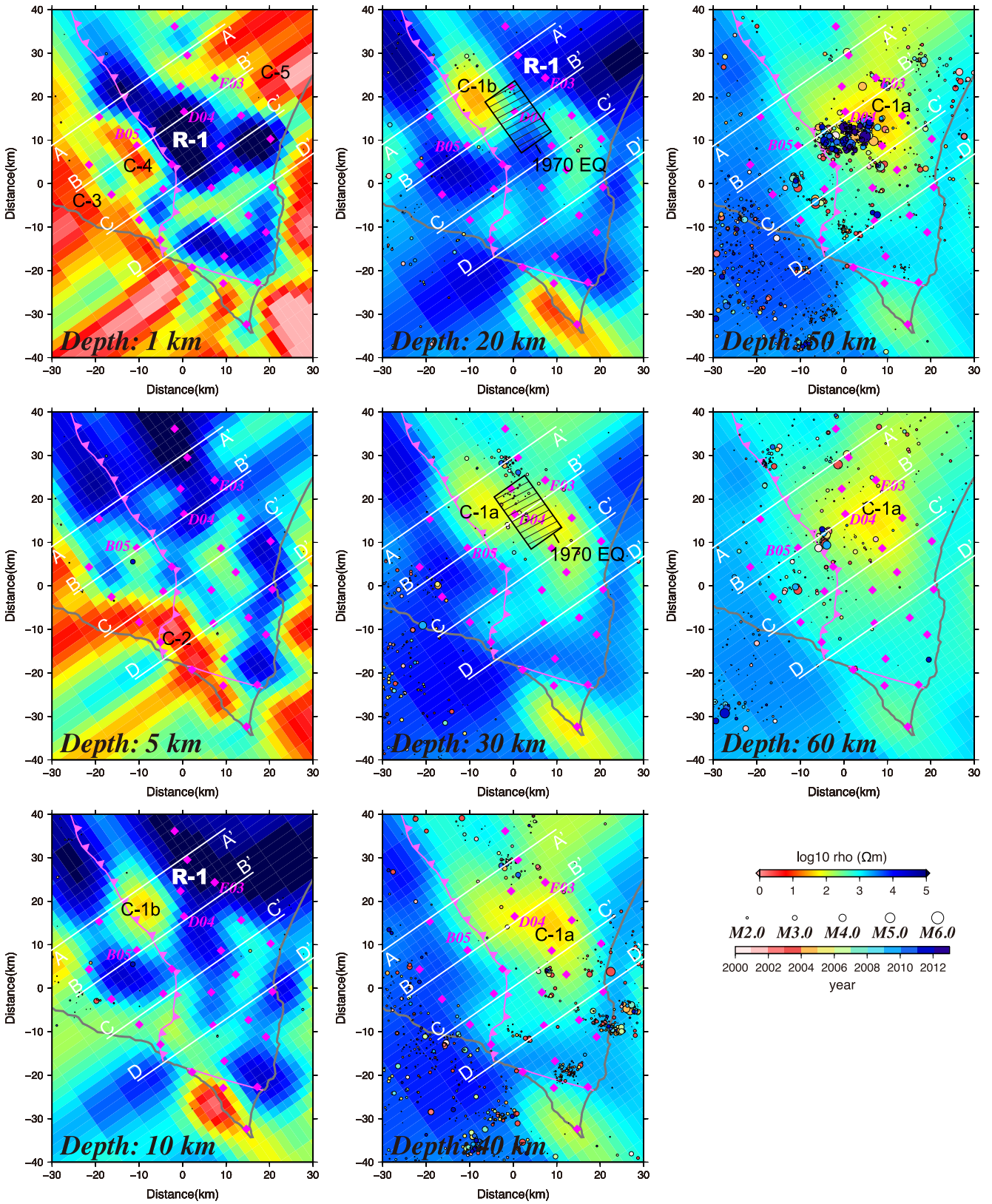

Figure 5. Horizontal resistivity cross sections from the inverted model. Diamonds denote MT sites. Gray and purple lines denote the coastline and Hidaka main thrust, respectively. Circles denote hypocenters of the Japan Metrological Agency between 2001 and 2012. Diamonds denote MT sites. The hatched area indicates the aftershock area of the 1970 Hidaka earthquake (M6.7) [*Moriya*, 1972].

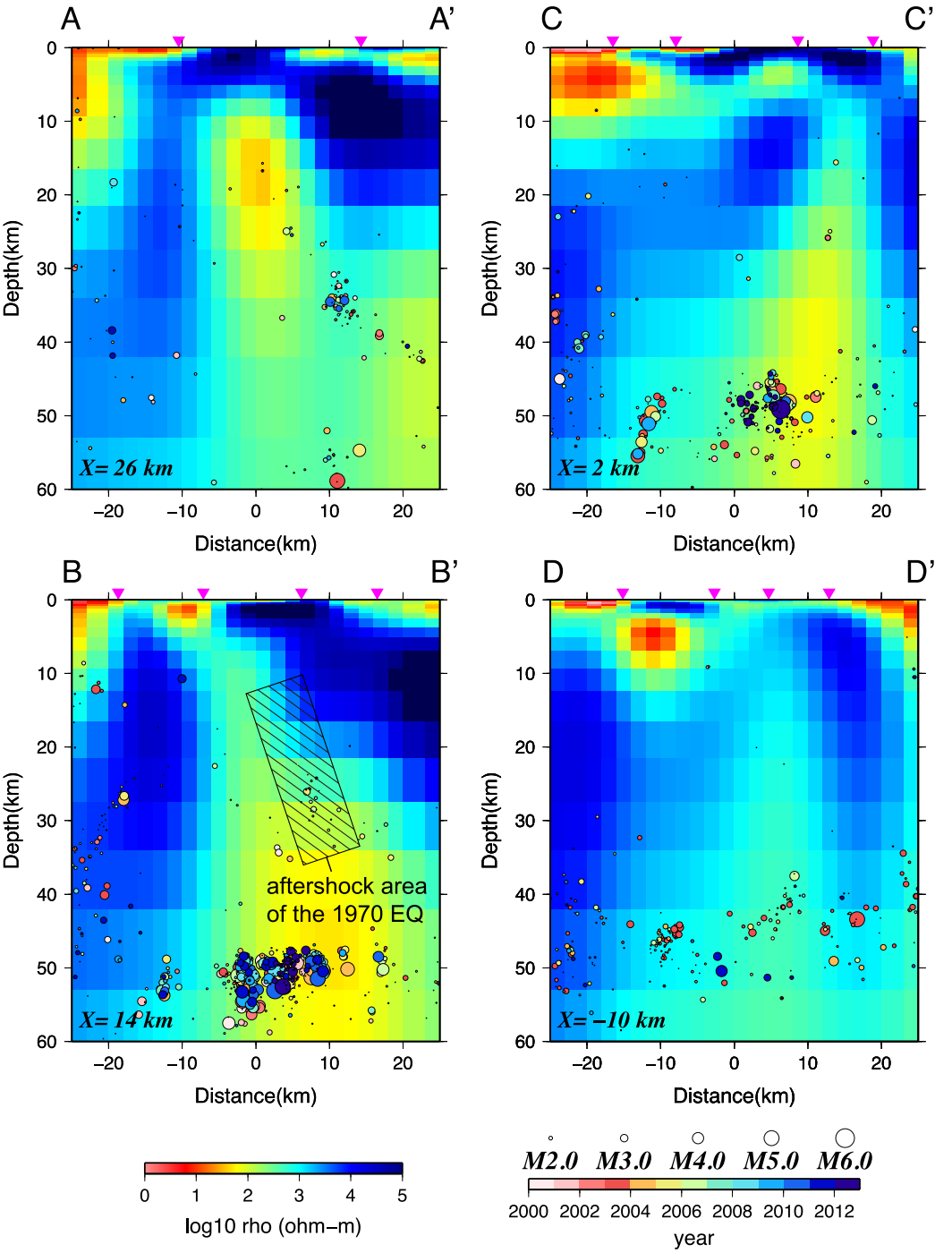

Figure 6. Vertical resistivity cross sections of the inverted model. Locations of the sections are shown as white lines in Figure 5. Symbols are the same as in Figure 5.

4.1.3. Conductive Sedimentary Rocks (C-3, C-4, and C-5)

The Yezo Group consisting of Cretaceous sedimentary rocks is distributed at the surface of C-3. Because the formation shows low resistivity between 0.3 and 10 Ω m [*Ichihara et al.*, 2008], C-3 probably reflects the Yezo Group. C-5 can also be interpreted as Cretaceous sedimentary rocks in the Hidaka belt (Nakanogawa Group) and Neocene sedimentary rocks embedded beneath the Tokachi Plain based on the geological distribution. The conductor C-4 can be interpreted as a Cretaceous accretionary complex in the Idon-nappu belt based on the spatial coincidence with the surface geological distribution (Figure 1) and seismic reflection profile [e.g.,

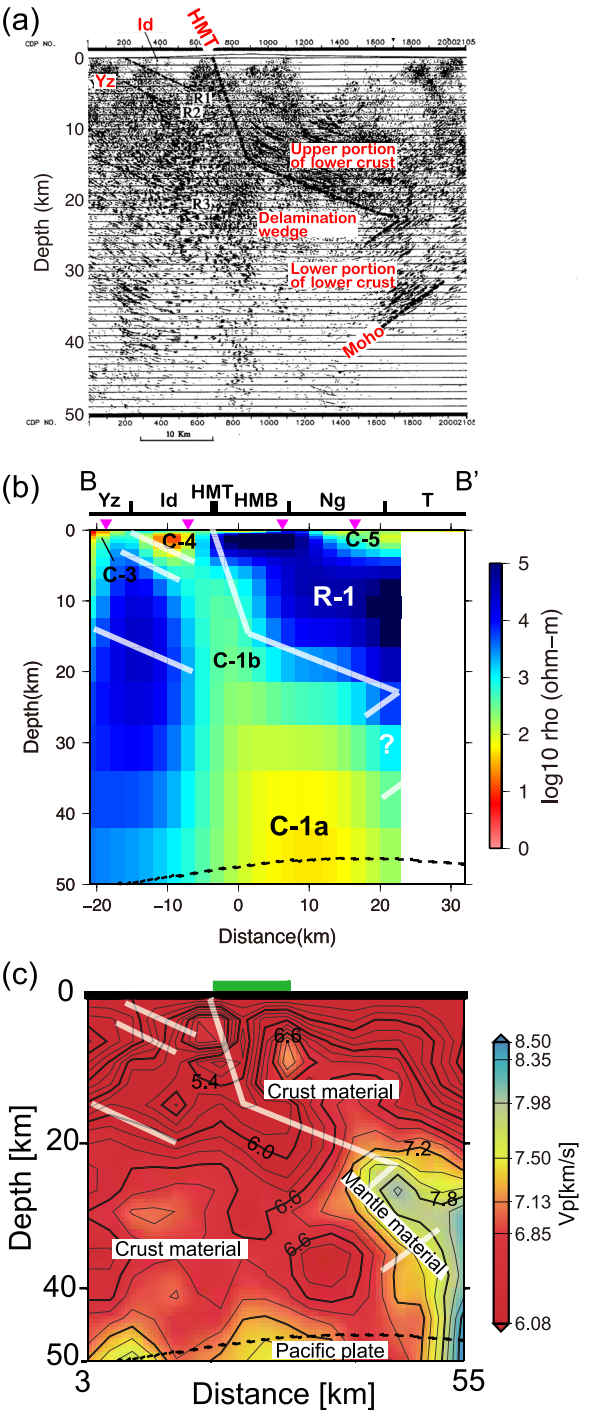

Figure 7. Comparison among the (a) seismic reflection [*Ito*, 2000], (b) resistivity (this study), and (c) P-wave velocity [*Kita et al.*, 2012] profiles beneath the B-B' line.

Ito, 2000] (Figure 7). Therefore, subsurface sedimentary rocks explain surface conductive areas in the southern part of the HCZ.

4.1.4. Resistivity Anomalies Beneath the Horoman Peridotite (C-2)

A high resistivity area (> 3,000 Ωm) was observed in the subsurface area (0–1 km depth) in the Horoman peridotite (Figures 1b, 5, and 6). It contacts with the metamorphic rocks in the Kurile arc (R-1) at the eastern margin. Because peridotites have high resistivity (3,000 Ωm) at the surface [*Palacky*, 1987], the subsurface high resistivity layer was interpreted as the peridotite rock body. However, the resistivity of the area of C-2 beneath the Horoman peridotite seems to be too low to be dry peridotite. Possible interpretations of C-2 are as follows: (1) peridotite is also distributed in the C-2 area, but pore fluid reduces the resistivity associated with serpentinization; and (2) sedimentary rocks such as C-3 and C-5 belonging to the NE Japan arc are distributed beneath the Horoman peridotite. This indicates that the rock body of Horoman peridotite is horizontally thin despite the fact that the rocks in the Hidaka metamorphic belt are highly inclined. This hypothesis constrains the process of uplift of the mantle material to the surface, although additional MT surveys and detailed analyses are required because the lack of MT measurements above the Horoman peridotite results in inadequate resolution of the resistivity image to allow more accurate interpretation (Figure 1b).

4.2. Implications for Earthquakes and Fluid Transportation

The fault-ruptured area of the 1970 Hidaka earthquake (M 6.7) was estimated to occur in the center of the HCZ at a depth of between 15 and 35 km based on the aftershock distribution (Figure 8) [*Moriya*, 1972]. *Kita et al.* [2012] estimated a reverse-fault mechanism with a strike along the NW–SE direction for the earthquake. They concluded that the fault plane was located along the boundary between the high- and low-velocity zones that was interpreted as the HMT. The location of the resistivity boundary between C-1b and R-1 was also located on the HMT, which supports *Kita et al.*'s [2012] conclusion that a section of the HMT served as part of the fault plane of the 1970 earthquake (Figure 8).

C-1a and C-1b were interpreted as an area with upwelling fluid from the subducting Pacific plate (see section 4.1.2). However, the fluid pathway was narrowed in the shallow area and is capped with Hidaka metamorphic rocks (R-1) near the surface. Thus, the upwelling fluid probably increases the pore fluid pressure and results in

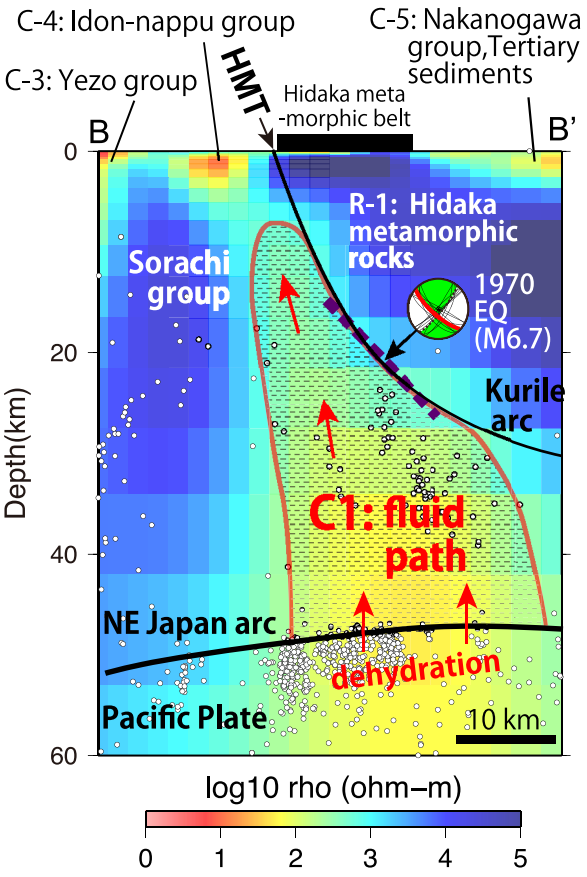

Figure 8. Interpretations of the resistivity model beneath the B-B′ line.

over-pressurized conditions in C-1b. Because over-pressurized pore fluid reduces shear strength and thus enhances fault slip under compressional stress conditions [*Scholz*, 2002], reverse-type fault rupturing was possible in the focal area of the 1970 Hidaka earthquake even in areas normally too deep to produce inland earthquakes in dry conditions. This mechanism may also explain the high seismicity observed in this area (Figure 6). Because pore fluid-rich areas have also been reported in other reverse-type active fault zones [e.g., *Ichihara et al.*, 2011], over-pressurized pore fluid may be a common feature that causes reverse-type inland earthquakes.

A high-seismicity area including the reverse-type fault earthquake of 25 August 2012 (M6.1) was displayed in the C-1a area where dehydration in the subducting oceanic plate supplies pore fluid to this area (Figures (5 and 6), and 8). Although the precise earthquake locations have not been determined, they would be expected to occur at the surface or within the upper oceanic crust of the subducting Pacific plate. Dehydration embrittlement is thought to be a cause of earthquakes under these tectonic conditions beneath the NE Japan arc [e.g., *Hacker et al.*, 2003]. In this case, dehydrated fluid also enhances seismic activity in the C-1a area. Therefore, the flow of upwelling fluid in the center of the collision zone originating from the deep plate boundary is possibly associated with seismic activity at various depths.

5. Conclusions

We conducted wideband and long-period MT surveys at 27 sites in the southern part of the HCZ and obtained resistivity models based on the 3-D inversion procedures. The inverted resistivity image showed a high-resistivity zone beneath the Hidaka Metamorphic Belt (R-1), a low-resistivity zone beneath the center of the HCZ that was distributed from near the surface to the subducting Pacific plate (C-1a and C-1b), a low-resistivity zone beneath the Horoman peridotite (C-2), and subsurface low-resistivity zones (C-3, C-4 and C-5).

These resistivity anomalies constrain the subsurface geology and fluid distribution beneath the arc-arc collision zone as follows: (1) C-1a and C-1b reflect the fluid pathway from the oceanic crust in the subducting Pacific slab; and (2) R-1 corresponds to the Hidaka metamorphic rock sequence. The location of the boundary between C-1b and R-1 is consistent with the Hidaka main thrust and supports the collision model that the upper-middle part of the crust in the Kurile arc obducted over the NE Japan arc. (3) C-2 may be related to the uplift process of mantle materials to the surface, although additional MT surveys are required. (4) C-3, C-5 and C-4 were interpreted as Cretaceous-Neocene conductive sediment rocks and accretionary complex based on their coincidence with the surface geology and active seismic surveys. The area of the anomalously deep inland earthquake (the 1970 Hidaka earthquake [M6.7]) is located on the edge of the pore fluid-rich zone (C-1b). Because the pore fluid reduces shear strength, the occurrence of C-1b is probably a cause of fault slip in this area. The high seismicity in C-1a may also be associated with dehydrated fluid. Therefore, the path of upwelling fluid within the arc-arc boundary probably enhances the seismicity.

Acknowledgments
The authors thank Hiroyuki Kamiyama, Venera Doblica and Takanori Kajiwara for setting up the MT instrumentation. We are also grateful to the landowners for their cooperation in establishing the MT observation stations. Constructive discussions with Dr. Saeko Kita, National Research Institute for Earth Science and Disaster Prevention, Japan, improved the content of manuscript. The authors also thank anonymous reviewers and editors for suggestions to improve the manuscript. The Kakioka Geomagnetic Observatory and Geographical Survey Institute, Japan, provided us their continuous geomagnetic records at Memanbetsu and Esashi stations, respectively, as remote references. For this study, we have used the computer systems of the Earthquake and Volcano Information Center of the Earthquake Research Institute,the University of Tokyo. Weerachai Siripunaraporn is thanked for supplying the WSINV3D code. Generic Mapping Tools software [*Wessel and Smith*, 1998] was used to produce some of the figures. All the magnetotelluric impedance tensors observed in this study are shown in the supporting information file (Figure S1); digital data including time series may be obtained from HI (email: h-ichi@maritime.kobe-u.ac.jp).

References

Arita, K., T. Ikawa, T. Ito, A. Yamamoto, M. Saito, Y. Nishida, H. Satoh, G. Kimura, T. Watanabe, T. Ikawa, and T. Koruda (1998), Crystal structure and tectonics of the Hidaka collision zone, Hokkaido (Japan), revealed by vibroseis seismic reflection and gravity surveys. *Tectonophysics*, *290*(3–4), 197–210, doi:10.1016/S0040-1951(98)00018-3.

Aizawa, K., et al. (2014), Three-dimensional resistivity structure and magma plumbing system of the Kirishima Volcanoes as inferred from broadband magnetotelluric data, *J. Geophys. Res. Solid Earth*, *119*, 198–215, doi:10.1002/2013JB010682.

Becken, M., and O. Ritter (2012), Magnetotelluric studies at the San Andreas Fault Zone: Implications for the role of fluids, *Surv. Geophys.*, *33*(1), 65–105.

Bertrand, E. A., M. J. Unsworth, C. W. Chiang, C. S. Chen, C. C. Chen, F. T. Wu, E. Turkoglu, H. L. Hsu, and G. J. Hill (2012), Magnetotelluric imaging beneath the Taiwan orogen: An arc-continent collision, *J. Geophys. Res.*, *117*, B01402, doi:10.1029/2011JB008688.

Caldwell, T. G., H. M. Bibby, and C. Brown (2004), The magnetotelluric phase tensor, *Geophys. J. Int.*, *158*(2), 457–469.

Chave, A. D., and D. J. Thomson (2004), Bounded influence magnetotelluric response function estimation, *Geophys. J. Int.*, *157*(3), 988–1006.

Fuji-ta, K., T. Katsura, and Y. Tainosho (2004), Electrical conductivity measurement of granulite under mid- to lower crustal pressure-temperature conditions, *Geophys. J. Int.*, *157*(1), 79–86.

Gamble, T. D., J. Clarke, and W. M. Goubau (1979), Magnetotellurics with a remote magnetic reference, *Geophysics*, *44*(1), 53–68.

Geological Survey of Japan (2007), Seamless digital geological map of Japan 1: 200,000. May 12, 2007 version, *Res. Inf. Database DB084*.

Hacker, B. R., S. M. Peacock, G. A. Abers, and S. D. Holloway (2003), Subduction factory—2. Are intermediate-depth earthquakes in subducting slabs linked to metamorphic dehydration reactions?, *J. Geophys. Res.*, *108*(B1), 2030, doi:10.1029/2001JB001129.

Ichihara, H., and T. Mogi (2009), A realistic 3-D resistivity model explaining anomalous large magnetotelluric phases: the L-shaped conductor model, *Geophys. J. Int.*, *179*(1), 14–17.

Ichihara, H., R. Honda, T. Mogi, H. Hase, H. Kamiyama, Y. Yamaya, and Y. Ogawa (2008), Resistivity structure around the focal area of the 2004 Rumoi-Nanbu earthquake (M 6.1), northern Hokkaido, Japan, *Earth Planets Space*, *60*(8), 883–888.

Ichihara, H., et al. (2011), A fault-zone conductor beneath a compressional inversion zone, northeastern Honshu, Japan, *Geophys. Res. Lett.*, *38*, L09301, doi:10.1029/2011GL047382.

Ichihara, H., T. Mogi, and Y. Yamaya (2013), Three-dimensional resistivity modelling of a seismogenic area in an oblique subduction zone in the western Kurile arc: Constraints from anomalous magnetotelluric phases, *Tectonophysics*, *603*, 114–122.

Ichihara, H., S. Sakanaka, M. Mishina, M. Uyeshima, T. Nishitani, Y. Ogawa, Y. Yamaya, T. Mogi, K. Amita, and T. Miura (2014), A 3-D electrical resistivity model beneath the focal zone of the 2008 Iwate-Miyagi Nairiku earthquake (M 7.2), *Earth Planets Space*, *66*(50), 1–9.

Ito, T. (2000), Crustal structure of the Hidaka collision zone and its foreland fold-and-thrust belst, Hokkaido, Japan [in *Japanese with English abstract], J. Jpn. Assoc. Pet. Technol.*, *65*(1), 103–109.

Iwasaki T., K. Adachi, T. Moriya, H. Miyamachi, T. Matsushima, K. Miyashita, T. Takeda, T. Taira, T. Yamada, and K. Ohtake (2004) Upper and middle crustal deformation of an arc-arc collision across Hokkaido, Japan, inferred from seismic refraction/wide-angle reflection experiments, *Tectonophysics 388* (1–4), 59–73.

Iwasaki T., O. Ozel, T. Moriya, S. Sakai, S. Suzuki, G. Aoki, T. Maeda, and T. Iidaka (1998) Lateral structural variation across a collision zone in central Hokkaido, Japan, as revealed by wide-angle seismic experiments. *Geophys J Int 132*(2), 435–457.

Kimura, G. (1986), Oblique Subduction and Collision - Fore-Arc Tectonics of the Kuril Arc, *Geology*, *14*(5), 404–407.

Kimura, G. (1994), The latest cretaceous early paleogene rapid growth of accretionary complex and exhumation of high-pressure series metamorphic rocks in northwestern Pacific Margin, *J. Geophys. Res.*, *99*(B11), 22,147-22,164.

Kita, S., T. Okada, A. Hasegawa, J. Nakajima, and T. Matsuzawa (2010), Anomalous deepening of a seismic belt in the upper-plane of the double seismic zone in the Pacific slab beneath the Hokkaido corner: Possible evidence for thermal shielding caused by subducted forearc crust materials, *Earth Planet. Sci. Lett.*, *290*(3-4), 415–426.

Kita, S., A. Hasegawa, J. Nakajima, T. Okada, T. Matsuzawa, and K. Katsumata (2012), High-resolution seismic velocity structure beneath the Hokkaido corner, northern Japan: Arc-arc collision and origins of the 1970 M 6.7 Hidaka and 1982 M 7.1 Urakawa-oki earthquakes, *J. Geophys. Res.*, *117*, B12301, doi:10.1029/2012JB009356.

Kita, S., J. Nakajima, A. Hasegawa, T. Okada, K. Katsumata, Y. Asano, and T. Kimura (2014), Detailed seismic attenuation structure beneath Hokkaido, northeastern Japan: Arc-arc collision process, arc magmatism, and seismotectonics, *J. Geophys. Res. Solid Earth*, *119*, 6486–6511, doi:10.1002/2014JB011099.

Komatsu, M., S. Miyashita, J. Maeda, Y. Osanai, and T. Toyoshima (1983), Disclosing of a deepest section of continental-type crust up-thrust as the final event of collosion of arcs in Hokkaido, North Japan, in *Accretion Tectonics in the Circum-Pacific Regions*, edited by M. Hashimoto and S. Uyeda, pp. 149–165, TERRAPUB, Tokyo.

Moriya, T. (1972), Aftershock activity of the Hidaka mountains earthquake of January 21, 1970, *J. Seismol. Soc. Jpn.*, *24*, 287–297.

Ogawa, Y., Y. Nishida, and M. Makino (1994), A collision boundary imaged by magnetotellurics, Hidaka Mountains, Central Hokkaido, Japan, *J. Geophys. Res.*, *99*(B11), 22,373–22,388.

Osanai, Y., K. Arita, and M. Bamba (1986), P-T conditions of granulite-facies rocks from the Hidaka metamorphic belt, Hokkaido, Japan [in Japanese with English abstract], *J. Geol. Soc. Jpn.*, *92*, 793–808.

Palacky, G. J. (1987), Resistiivty characteristics of geologic targets, in *Electomagnetic Method in Applied Geophysics––Theory*, edited by M. N. Nabighian, pp. 53–129, Soc. of Explor. Geophys., Tulsa, Okla.

Scholz, C. H. (2002), *The Mechanics of Earthquakes and Faulting*, 2nd ed., 471 pp., Cambridge Univ. Press, Cambridge, U. K.

Shiina, T., J. Nakajima, G. Toyokuni, and T. Matsuzawa (2014), Guided wave observations and evidence for the low-velocity subducting crust beneath Hokkaido, northern Japan, *Earth Planets Space*, *66*(69), 1–10.

Sibson, R. H. (2014), Earthquake rupturing in fluid-overpressured crust: How common?, *Pure Appl. Geophys.*, *171*(11), 2867–2885.

Siripunvaraporn, W., and G. Egbert (2000), An efficient data-subspace inversion method for 2-D magnetotelluric data, *Geophysics*, *65*, 791–803.

Siripunvaraporn, W., M. Uyeshima, and G. Egbert (2004), Three-dimensional inversion for Network-Magnetotelluric data, *Earth Planets Space*, *56*(9), 893–902.

Takahashi, N. (1992), Evidence for melt segregation towards fractures in the horoman mantle peridotite complex, *Nature*, *359*(6390), 52–55.

Tsumura N., H. Ikawa, T. Ikawa, M. Shinohara, T. Ito, K. Arita, T. Moriya, G. Kimura, T. Ikawa (1999) Delamination-wedge structure beneath the Hidaka Collision Zone, central Hokkaido, Japan inferred from seismic reflection profiling. *Geophys Res Lett.*, *26*(8):1057–1060. doi: 10.1029/1999gl900192.

Unsworth, M. (2010), Magnetotelluric studies of active continent-continent collisions, *Surv. Geophys.*, *31*(2), 137–161.

Wannamaker, P. E., T. G. Caldwell, G. R. Jiracek, V. Maris, G. J. Hill, Y. Ogawa, H. M. Bibby, S. L. Bennie, and W. Heise (2009), Fluid and deformation regime of an advancing subduction system at Marlborough, New Zealand, *Nature*, *460*(7256), 733-U790.

Wessel, P., and W. H. F. Smith (1998), New, improved version of Generic Mapping Tools released, *Eos Trans. AGU*, *79* (47), 579.